30th Anniversary
Langmuir

Article

Growth and dissolution of calcite in the presence of adsorbed stearic acid

Maria Ricci, Juan José Segura, Blake Erickson, Georg Fantner, Francesco Stellacci, and Kislon Voitchovsky

Langmuir, **Just Accepted Manuscript** • DOI: 10.1021/acs.langmuir.5b01732 • Publication Date (Web): 18 Jun 2015

Langmuir is published by the American Chemical Society. 1155 Sixteenth Street N.W., Washington, DC 20036

Growth and dissolution of calcite in the presence of adsorbed stearic acid

Maria Ricci[1], Juan José Segura[1,§], Blake W. Erickson[2], Georg Fantner[2], Francesco Stellacci[1,2], Kislon Voïtchovsky[1, 3,*]

[1] Department of Materials Science and Engineering, École Polytechnique Fédérale de Lausanne (EPFL), 1015 Lausanne, Switzerland

[2] Interschool Institute of Bioengineering, École Polytechnique Fédérale de Lausanne (EPFL), 1015 Lausanne, Switzerland

[3] Department of Physics, Durham University, South Road, Durham DH1 3LE, UK

Abstract

The interaction of organic molecules with the surface of calcite plays a central role in many geochemical, petrochemical and industrial processes and in biomineralization. Adsorbed organics, typically fatty acids, can interfere with the evolution of calcite when immersed in aqueous solutions. Here we use atomic force microscopy in liquid to explore in real-time the evolution of the $(10\bar{1}4)$ surface of calcite covered with various densities of stearic acid and exposed to different saline solutions. Our results show that the stearic acid molecules tend to act as 'pinning points' on the calcite's surface and slow down the crystal's restructuring kinetics. Depending on the amount of material adsorbed, the organic molecules can form monolayers or bilayer islands that become embedded into the growing crystal. The growth process can also displaces the organic molecules and actively concentrate them into stacked multilayers. Our results provide molecular-level insights into the interplay between the adsorbed fatty acid molecules and the evolving calcite crystal, highlighting mechanisms that could have important implications for several biochemical and geochemical processes and for the oil industry.

Keywords: calcite, calcium carbonate, stearic acid, atomic force microscopy, brine, crystal growth, dissolution, adsorption from solution,

1. Introduction

Calcite (calcium carbonate, chemical formula $CaCO_3$) is among the main components of the earth's crust where it can primarily be found in sedimentary rocks such as limestone.[1] It is also the main constituent of the shells of marine organisms, and its relative abundance is largely linked to biomineralization.[2,3] Calcite can grow or dissolve rapidly depending on its environment[4], and plays a fundamental role in preserving the biosphere through its ability to regulate ocean acidification.[5] The dynamics of the physico-chemical transformations occurring at its surface is also key to countless industrial processes, for example in the polymer industry,[6] cement manufacturing,[7] nuclear waste storage,[8,9] waste water treatment[10], and in the petroleum industry, given its natural abundance in oil reservoirs[11].

In many natural and industrial processes, calcite is out of equilibrium with its surroundings and its surface morphology evolves rapidly, often in direct contact with ions and large organic molecules such as fatty acids that can influence calcite's fate.[12,13] During biomineralization, acidic organic macromolecules present in solution or on a contacting polymeric matrix can influence the nucleation and growth of the mineral.[12,14,15] In calcareous oil reservoirs, fatty acids also play an important role and are often used to model the heavy organics interaction with calcite's surface during oil recovery.[16,17] Aqueous solutions with various salt contents are usually injected into the reservoir to further enhance recovery[18-20], inducing a complex interplay between ions, organics and calcite.

At the present time, a molecular understanding of these processes remains challenging, first due to the highly dynamic nature of calcite when out of equilibrium with the contacting aqueous solution, but also due to the fact that the interactions between fatty acids and calcite are mediated by specific ions[14] that can themselves interfere with the kinetics of calcite restructuring[21-28]. Several studies have examined the interaction of organic molecules with calcite's surface under different circumstances,[29-31] but the inherent complexity of the system and the large number of variables able to influence calcite's surface dynamics often result in conflicting findings.[23,32]

Here we use high-resolution amplitude-modulation atomic force microscopy (AM-AFM) in liquid[33,34] to follow in real-time and with nanometer precision the evolution of calcite $(10\bar{1}4)$ coated with stearic acid (SA) and exposed to different saline solutions. Calcite could grow or dissolve, depending on the ionic content of the solution (referred to as 'brines').

Our results show a rearrangement of the adsorbed SA layer driven by minimization of the hydrophobic contact with the solution, and a restructuring of calcite around the adsorbed organic patches that become trapped into a growing crystal. SA patches act as 'pinning points' precluding crystal growth and dilution along preferential crystallographic directions, similarly to other organics.[30,35] Depending on the amount of organic coverage the growth process can effectively concentrate the SA in confined areas. Significantly, our results suggest

that the restructuring of calcite's surface is an important mechanism determining the fate of adsorbed organics, including in oil-related application.[36]

2. Materials and Methods

2.1 Sample preparation

Clear, optically transparent calcite crystals originating from Mexico (Crystals, Rocks and Gems, Denver, CO, USA) were used for this study. The calcite samples were attached on a metallic disk (SPI Supplies, West Chester, PA 19380, USA) with 5 min epoxy glue (Araldite, Denver, USA) and subsequently cleaved with a razor blade to expose the $(10\bar{1}4)$ surface. The cleavage of the samples was conducted after the glue had cured so as to expose a fresh calcite surface. This strategy avoided contamination of the surface and provided a good stability during AFM experiments.

Immediately after cleaving, the samples were either imaged in the desired brine concentration or exposed to a vapor of SA (Sigma Aldrich, St Louis, MO 63103, USA) in order to create the desired adsorbed SA layer. For the SA deposition, 2 mg of SA were placed into a 2 ml glass vial and capped with Teflon tape. The tape was punctured in a single location and the vial subsequently heated to 120°C for at least 15 minutes. A calcite crystal was positioned above the punctured hole to expose the freshly cleaved surface to the SA hot vapor. Different coverage of SA on calcite were obtained by tuning the deposition temperature, the dimension of the hole in the Teflon tape, the depth of the glass vials and the exposure time. Calibration of the deposition process could be achieved by setting temperature and hole size, and imaging a samples series in air for various exposure times. The SA evaporation technique allowed the best control of the surface coverage and minimized the presence of unadsorbed SA in the imaging solution, after subsequent immersion of the sample into a brine. Despite these advantages, the technique does not reflect fatty acid adsorption in natural environment such as oil reservoirs or during biomineralization where the adsorption takes place directly into the aqueous solution. We therefore also tested a so-called 'two-phases' preparation method that better mimics situations in which organic and aqueous phase are directly mixed together. This was carried out as a control and the details of the method as well as the related experimental results are presented in section 2 of Supporting Information. In short, two immiscible solvents, water and chloroform, are mixed together. The SA was dissolved in the chloroform phase. Freshly cleaved calcite crystals were immersed into the heated mixture and subsequently removed and rinsed with ultrapure water (Milli-Q, 18.2 ΩM, <4 ppm TOC,

Merck-Milipore, Billerica, MA, USA). The two-phases method provided similar results as the evaporation method.

In both preparation methods, the SA is adsorbed to the surface of calcite before immersion into the relevant brine and no SA should be left in the solution, except for potential SA desorption from the surface. Since the AFM images reveal stable organic patches throughout most experiments, the formation of calcium stearate in solution can be neglected.

2.2 Brines preparation

In nature as well as in industry, the composition of the brines (saline solutions) in contact with calcite usually depends on practical issues such as the ground geology and composition, and the quality of the water available. Brines can hence vary substantially between situations, with in some cases, certain ions present in the brine able to strongly interfere with the growth and dissolution process of calcite.[21-28] We have therefore selected two distinct brines, choosing their ionic content based on their expected ability to interfere weakly (Brine1) or strongly (Brine2) with calcite's evolution. In each case, the brines were progressively diluted from an initial supersaturated salt composition so as to allow the study of both calcite growth and dissolution in the presence of SA and the relevant ions. The ionic species used in our brines are found in most natural systems but their relative ratio often varies. We used a composition suggested by Shell Global Solutions International and that reflects typical ionic compositions used in reservoir flooding. The results should nonetheless remain generally valid for most natural systems.

The supersaturated brines were prepared by dissolving the desired amount of salts (Sigma Aldrich, St Louis, MO 63103, USA) in ultrapure water. The composition of the brines is detailed in Table 1. Hereafter we consistently refer to them as Brine1 and Brine2, respectively.

	Brine1 (g/l)	Brine2 (g/l)
NaCl	164.64	164.64
KCl	0.95	0.95
$CaCl_2 \times 2\ H_20$	60.81	60.81
$MgCl_2 \times 6\ H_20$	18.63	18.63
$SrCl_2 \times 6\ H_20$	-	3.96
$Na_2SO_4 \times 10\ H_20$	0.67	0.67
$NaHCO_3$	0.12	0.12

Table 1: Composition of the two brines used in this paper. The salt concentrations are given in g/l. The calculated saturation index and measured pH are respectively 0.99 and 6 (Brine 1) and 0.98 and 6 (Brine 2). The given saturation index are for calcite, but other polymorphs such as aragonite, dolomite,

and strontianite (only Brine 2) can in principle form (see Fig. 1 and section 1 of the Supporting Information for details).

Subsequent dilutions of the brines were conducted with ultrapure water. Diluted brines are consistently referred to by their degree of dilution, for example Brine1_×20 for a 20 times dilution of Brine1. The fate of a calcite sample immersed into a given brine dilution can be predicted from the brine's saturation index (SI), defined as the logarithm of the ratio between the Ion Activity Product (IAP) and the equilibrium constant (KT) of the mineral phase considered. Negative SI correspond to unsaturated solutions with respect to the mineral while positive values correspond to supersaturated solutions. At SI=0 the crystal is at equilibrium with the brine. The SI can be calculated for each solution using the PHREEQC software[37] (see section 1 of the Supporting Information for details on each experiment). A plot of the SI for the different dilutions of Brine 1 and Brine 2 used in this study is presented in figure 1.

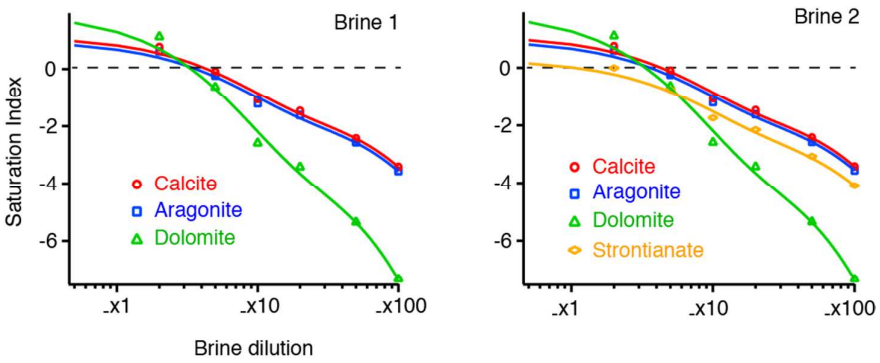

Figure 1: Evolution of the SI for each brine upon dilution. The points have been calculated using PHREEQC for each dilution studied, and the curves were obtained by fitting. A SI curve is given for each of the main calcium carbonate polymorphs susceptible to grow/dissolve in the brine considered. The dotted horizontal line indicate the equilibrium point with growth and dissolution occurring for SI values above, respectively below the line.

2.3 Atomic Force Microscopy

All samples were investigated at room temperature first in air and then in liquid, unless specified otherwise. The work was conducted on commercial atomic force microscopes (AFM)s. Different AFMs were used, depending on the type of measurement conducted.

Imaging conditions used for the AM-AFM experiments

When operated in amplitude-modulation (AM), the AFM cantilever is oscillated near its resonance frequency and the oscillation amplitude of the tip is kept constant by a feedback

loop that readjusts the tip-sample distance while scanning. A topographic image of the sample is obtained from the applied feedback correction in each point of the sample. The phase lag between the driving and the actual tip oscillations is left to vary freely and can be used to gain complementary (chemical or physical) information about the sample, depending on the imaging conditions.[33,38-40].

High-resolution images in liquid were obtained with typical working amplitudes A kept between 1 nm and 1.5 nm (peak-peak). The setpoint ratio A/A_0 was kept as large as possible (typically > 0.8) where A_0 is the free vibration amplitude of the lever in the liquid far from the surface. These operating conditions allow the AFM tip to probe mainly the interfacial liquid at the surface of the sample, without significantly interacting with the solid itself.[33,34,39,41,42] In this regime, the phase images provide indications about the local solvation free energy of the sample with darker contrasts indicating local maxima.

Lower resolution images tracking large (> 100 nm) regions of the sample necessitated larger free amplitude (>2 nm) and lower ratio A/A_0 (normally < 0.8) in order to better track the rough surfaces. In these conditions the interpretation of the phase signal is not straightforward, but often dominated by the contact mechanic between the tip and the sample, and hence variations in stiffness and viscosity of the material.[40,43,44]

Most of the experiments, in particular the results presented in Figures 2 and 4 were carried out in AM ('tapping' in the AFM commercial software) with a Multimode Nanoscope IIIA (Digital Instruments, now Brucker, Santa Barbara, CA, USA) equipped with an external lock-in amplifier. The measurements were conducted in a liquid cell using silicon nitride cantilevers (RC800-PSA, Olympus, Japan) with a nominal stiffness k_c = 0.76 N/m.

First images were acquired in air to estimate the surface coverage of organic molecules. The desired brine was subsequently injected into the fluid cell and the sample imaged in liquid without changing the tip. Using a home-built syringe system it was possible to exchange the liquid and progressively dilute the concentration of the brine without disengaging the sample. The evolution of the sample was followed in real time over a same area. During the liquid exchange process, the tip was lifted a few microns above the surface (z-piezo retraction) to prevent possible tip damage, but not disengaged. High resolution images of calcite surface could be routinely obtained, using a procedure and imaging conditions described above.[33,34,41,42] Occasionally, water evaporation from the imperfectly sealed liquid cell induced concentration of the imaging brine and a small shift between predicted and observed behavior of calcite in long dilution experiments (dilution and growth, as predicted by PHREEQC, see Supporting Information section 1). Since our experiments focus on trends in the evolution of calcite's surface, the results obtained with this AFM remains fully valid. Nonetheless, this limitation could be overcome using the perfectly sealed environmental chamber of a Cypher ES AFM (Asylum Research, Oxford Instrument, Santa Barabara, CA,

USA). The results presented in Figures 5 and 6 were performed in AM with a Cypher ES equipped with photothermal excitation (BlueDrive) and the same type of cantilevers as used on the Multimode Nanoscope IIIA.

Image analysis was performed with the software Gwyddion (http://gwyddion.net) and SPIP (Image Metrology, Denmark).

PeakForce Quantitative Nanomechanical Property Mapping

PeakForce Quantitative Nanomechanical Property Mapping (QNM) measurements (Figure 2) were performed on a Veeco Multimode 5 system equipped with a 10×10×2.5 μm scanner. The deflection sensitivity of the cantilever (Scanasyst-fluid, Bruker, Santa Barbara, CA, USA) was calibrated before the experiment and the cantilever's spring constant was obtained from its thermal spectrum in air.[45] In QNM mode, the tip-sample distance is modulated periodically at a frequency well below the cantilever's resonance frequency (typically at 1-2 kHz). When the tip is far away from the sample, the tip motion due to this oscillation is purely harmonic. When the tip scans the sample, it periodically 'taps' it. Being far form the cantilever's resonance, each tap acts can be seen as a standard nano-indentation experiment. Taking into account the harmonic motion of the base of the cantilever, it is possible to reconstruct 'on the fly' a standard set of force-distance curves for each tap.[46-48] The maximum indentation force exerted by the tip on the sample during each tap is called 'peak force' and used as a feedback parameter to achieve a topographic image.

The force curves can subsequently be used to deduce the tip indentation depth into the sample, the sample's Young modulus and the tip-sample adhesion upon retraction. These calculations are also done 'on the fly' for each tap by the AFM electronics. The tip indentation, sample elasticity and tip-sample adhesion maps are obtained simultaneously, as visible in Figure 3.

3. Results and Discussion

3.1 Reference experiments

Differential growth of SA free calcite in the two brines

In order to establish a reference point for the study, we investigated the evolution of pure calcite (i.e. without any SA coverage) in the supersaturated brines. When immersing calcite into a particular brine, the fate of the crystal can be predicted by calculating the brine's saturation index, SI, with respect to calcite (see section 2.2): a positive SI entails growth of the crystal while dissolution occurs for negative SI. At SI=0, calcite is at equilibrium with the

brine and the surface is stable, apart for possible restructuring. The same concept is sometimes described by the so-called 'scaling tendency' of the brine. Here, the SI has been calculated for each brine dilution studied using the PHREEQC[37] software (see section 1 of the Supporting Information).

The undiluted brines (Brine1_×0 and Brine2_×0) each have a positive SI and time-lapse AFM images over a same area show clear calcite growth in both cases (Figure 2). When observed at a same scale, the growing monoatomic steps are more regular in Brine1 (Figure 2A-B) than in Brine2 (Figure 2D-F) where the steps tend to form branched structures due to the presence of $SrCl_2$.

At high saline concentrations (down to _×2 diluted brines), not only calcite but also Aragonite ($CaCO_3$), Dolomite ($CaMg(CO_3)_2$) and Strontianite ($SrCO_3$, only in the case of Brine2) can in principle form (see Supporting Information). Given the presence of a preexisting calcite crystal, the new material growing on the surface is likely to be mostly calcite but Mg^{2+} and Sr^{2+} ions tends to enhance the formation of otherwise less stable aragonite and their presence in the newly formed crystal cannot be excluded.[24] Generally, impurities can have two possible effects on the growth process, depending on the model considered: the *impurity-incorporation* model assumes that the impurities are simply incorporated into the crystal during its growth[26] while the *step-pinning* model predicts a decrease of the advancing steps' velocity due to impurities adsorbing at step-edges. Mg^{2+} ions have been shown to obey to the first model[24], allowing the formation of relatively regular steps (Figure 2A-B). In contrast, Sr^{2+} ions follow the *step-pinning* model, resulting in a highly irregular growth process[22] as visible in Figure 2D-E. Both ions are, to a certain extent, incorporated in the newly formed crystal[47].

Experiments conducted in Brine1 and Brine2 allow us to explore the two main restructuring routes for calcite's surface in the presence of adsorbed SA.

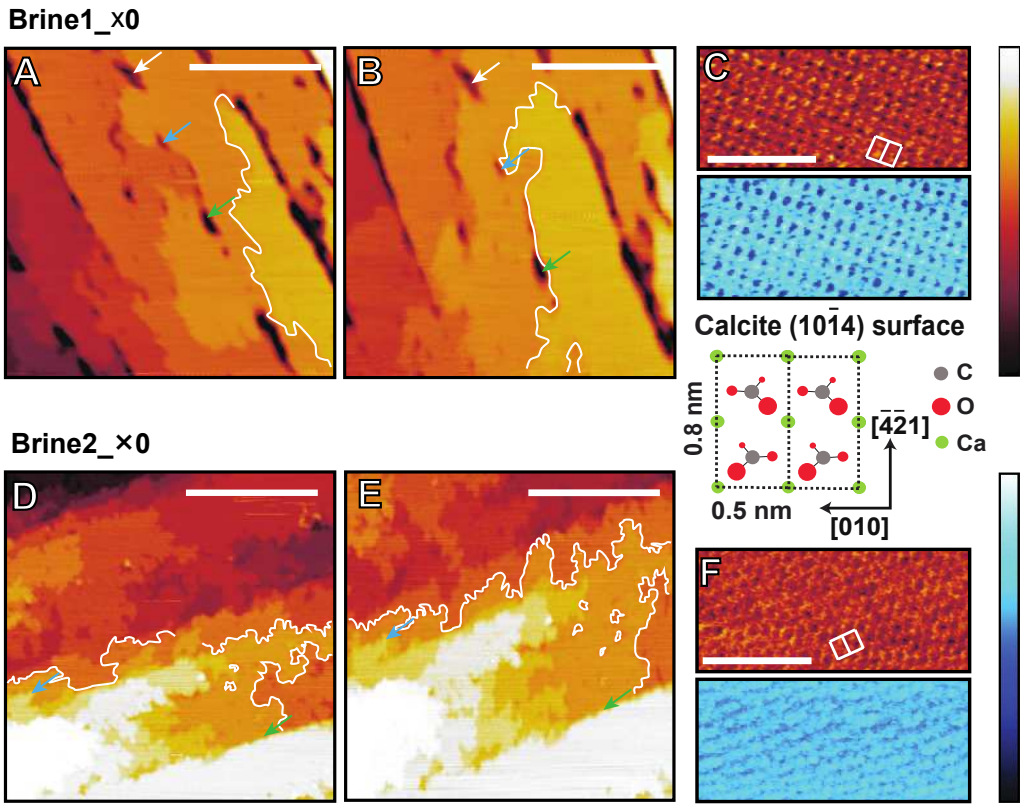

Figure 2: Step growth on calcite (10$\bar{1}$4) imaged by AM-AFM in Brine1_×0 (A-C) and Brine2_×0 (D-F). Time-lapse topographic images (2 min) show the advancing steps (A-B) and (D-E). In each case a same step is highlighted before and after growth has taken place, and each colored arrows indicate a same reference location on the surface to help visual inspection despite thermal drift. (C) and (F) are high-resolution topographic (brown scale) and phase (blue scale) images of calcite (10$\bar{1}$4) revealing the well-known atomic arrangement of the surface. Two unit cells are highlighted in each case. The scale bars are 200 nm (A, B, D, E) and 4 nm (C, F). The color scale bars are 3.5 nm (A, B, D, E), 0.4 nm (C, F) and 11° (C, F). The images are not drift corrected.

Structure of the SA patches at the surface of calcite in air and in liquid

An additional reference experiment is necessary in order to unambiguously interpret AFM images over SA-coated samples and determine which region of the sample's surface corresponds to calcite and which to adsorbed SA molecules. This experiment is needed because SA domains can become embedded into the crystal after exposition to supersaturated brines, and topography alone may therefore not be sufficient as a differentiation criterion. Here differentiation was achieved using quantitative nanomechanical property mapping (QNM, see methods). QNM can simultaneously map topography, deformation and the adhesion force experienced by the scanning tip when touching the sample. SA-coated samples were first imaged in air and subsequently in Brine2_×2 (Figure 3). The dilution was chosen to minimize calcite growth and hence help result interpretation.

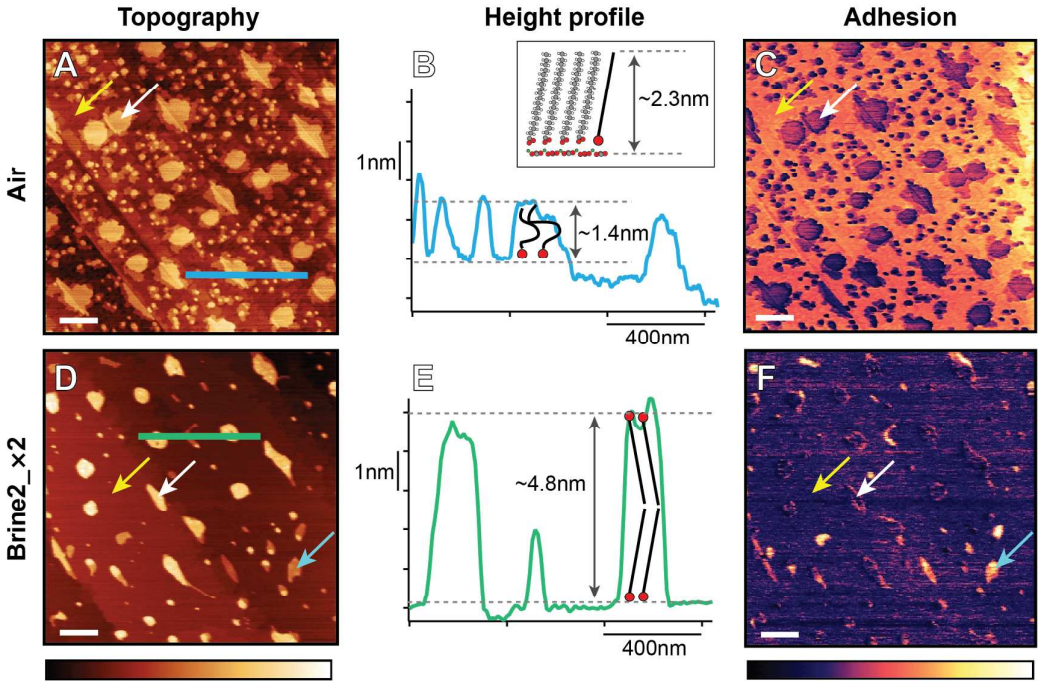

Figure 3: QNM measurements on a calcite surface partially covered with SA molecules showing topography (A, D) and tip-sample adhesion (C, F). The sample is measured first in air (A-C) and subsequently in Brine2_×2 (D-F) with a same tip. The yellow and white arrows in (A) and (C) indicate free calcite and SA-covered regions respectively, with an adhesion contrast of 19.7±0.2% (see section 4 of the Supporting Information). The blue horizontal line in (A) corresponds to the height profile in (B). The yellow, white and blue arrows in (D) and (F) indicate free calcite, multilayer SA-covered and monolayer SA-covered regions respectively. The difference in measured adhesion between calcite and multilayer covered calcite is statistically negligible (7±53%), indicating that the SA patches expose their hydrophilic heads. In contrast, occasional SA monolayers exposing their hydrophobic tails induce a 215±96% adhesion contrast (F). The green horizontal line in (D) corresponds to the height profile in (E). For each profile (B, E), the presumed molecular arrangement of the adsorbed SA molecules is presented, assuming a 2.3 nm thickness for a densely packed SA monolayer (inset).[51] The scale bars are 400 nm (A, C, D, F). The color scale bars are 4 nm (A), 21.8 nN (C), 9 nm (D) and 1.1 nN (F). See Figure S3 for more details.

In air (Figure 3A-C), the SA patches appear brighter in topography and induced a lower (darker) tip-surface adhesion compared to bare calcite surface. Capillary forces dominate the adhesion between the hydrophilic tip and the sample, and the tip consistently experiences a higher adhesion force over the hydrophilic calcite surface than over the hydrophobic alkyl chains exposed by SA patches.[50] The SA patches appear irregular in shape and thickness (Figure 3A, B), but they are stable in time. The typical thickness of a patch varies between 1.1 nm and 1.4 nm, depending on imaging conditions. Quantification of the tip mechanical indentation (Figure S3) indicates a similar indentation depth everywhere on the sample,

confirming that the measured SA layer thickness is reliable. This thickness value is lower than the 2.3-2.4 nm expected for a densely packed SA monolayer in standing up phase.[51,52] We explain the apparent reduced SA height by loose and disordered molecular packing on the surface (Figure 3B). Similar results have been previously reported for SA adsorbed on calcite[53] and on different substrates,[52,54] and explained by a tilt or partial horizontal arrangement of the SA alkyl chains. The presence of a completely 'lying down' SA phase in Figure 3A-B can be excluded since it would appear thinner than measured.

After immersion of the sample into Brine2_×2, SA patches appear taller and better defined, with a thickness corresponding to densely packed SA multilayers (generally between 2 to 4 layers, see also Figure S4). This indicates a water-induced reorganization of the SA molecules driven by minimization of the alkyl tails' hydrophobic exposure. Very little contrast in the tip-sample adhesion force is visible between SA and calcite regions (yellow and white arrows in Figure 3D and 3F), confirming that most SA regions expose the molecules' hydrophilic heads to the liquid. A few exceptions can be found (blue arrow, Figure 3D and 3F) where thinner patches occasionally still expose their hydrophobic alkyl chains, which results in a particularly low tip-sample adhesion. The brine induces a rearrangement of adsorbed SA molecules driven by a minimization of the hydrophobic exposure. The rearrangement creates predominantly bilayers and occasionally densely packed monolayers, even if the initial adsorbed SA layer is not completely formed.

3.2 Dissolution and growth of calcite with low SA coverage.

Calcite samples partially covered with SA (Figure 3) were first immersed into the supersaturated brines, inducing crystal growth around the SA patches. The process is illustrated in figure 4A-B for Brine1_×2.

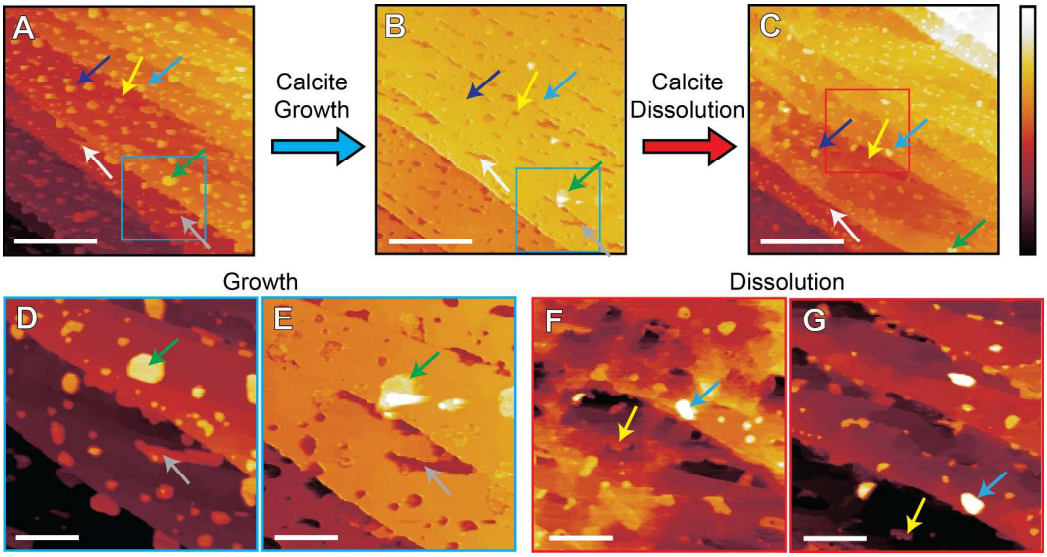

Figure 4: Calcite growth and subsequent dissolution observed over a same region partially covered with SA patches in Brine1. Each colored arrows indicate a same SA patch throughout the growth and dissolution processes. (A) Topographic image of the sample taken immediately after the injection of supersaturated Brine1_×2. The sample was left for 1 h 44 min in Brine1_×2 and subsequently for 39 min in Brine1_×5 allowing the crystal to grow. Brine1_×10 is then injected to reverse the growth process and an image of the same area as (A) is acquired immediately after injection (B). Further dissolution of the surface is observed 1 h 7 min after injection of Brine1_×50 (C). (D) and (E) are magnification of (A) and (B) respectively. (F) is a magnification of (C) with subsequent further dilution in Brine1_×100 (G). All images are topographic images. The scale bars are 1 µm (A-C) and 250 nm (D-G). The color scale bars are 20 nm (A-E) and 10 nm (F, G). A more detailed description of the process is available in Figures S1 and S6.

The SA patches, initially protruding from the surface (arrows in Figure 4A) progressively turn into apparent holes (Figure 4B), as the crystal grows around them. The process can be reversed upon subsequent dilution of the brine, recovering the organic patches embedded inside the rock (Figure 4B). The SA patches remain stable throughout the crystal growth and dissolution processes that they tend to slow down. The initial growth phase proceeds from step-edges and tend to level the surface, which becomes flatter and more regular. As a result, SA patches located at the base of steps are first incorporated into the crystal while patches located above the highest steps maintain longer their protruding aspect (arrows in Figure 4A-B and D-E). The subsequent brine dilution recovers the initial surface, including the embedded SA patches (arrows in Figure 4B-C and F-G).

A very similar trend can be observed in Brine2, with details of the dissolution process presented in figure 5.

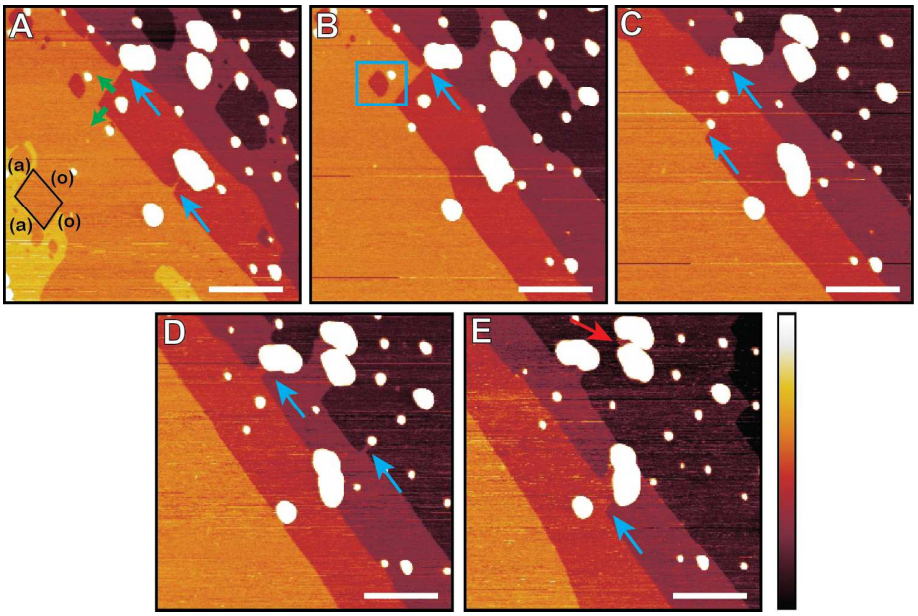

Figure 5: Dissolution of calcite partially covered with SA in Brine2_×20. (A) Initial surface immediately after injection of the diluted brine. The same area is imaged after 4 min (B), 8 min (C), 13 min (D) and 21 min (E). The obtuse and acute steps are indicated respectively as (o) and (a) in (A). The green arrows in indicate the preferential directions for calcite dissolution and the sketch on the left represent a typical etch pit, as exemplified in the blue box in (B). The blue arrows indicate pinning points and the red arrow in (E) indicates an 'artificial' terrace, stabilized by SA patches. The scale bar is 250 nm and the color scale bar 2 nm in all images. All images are topographic images.

Adsorbed SA molecules effectively act as pinning points during the growth and dissolution of calcite, similarly to Sr^{2+} ions. Consecutive images of a same area in Brine2_×20 (blue arrows in Figure 5) shows that the organic patches pin the dissolving steps. This is consistent with previous findings that showed organics to act as a growth inhibitor for calcium carbonate.[30,55] Molecular dynamic simulations found that the carboxylic acid acts as a growth inhibitor due to its ability to replace water molecules at calcite steps, effectively blocking the access for new growth material.[35] Here we observe faster calcite dissolution along acute (a) steps than along obtuse (o) steps[56] (Figure 5A), but a clear quantification of this differential dissolution is challenging given its dependence on the brine concentration[26] and the presence of adsorbed organics that can interfere with the process. This faster calcite dissolution along acute (a) steps contradicts the usual trend reported for calcite dissolution[26,56], but similar observations have been reported[23] in the presence of Mg^{2+}, even at very low concentrations.[32] Other ions present in the brine can affect the surface restructuring dynamics with K^{+} increasing the spreading rate of both acute and obtuse steps[28] and SO_4^{2-} inducing an elongation of the etch pits[57], but Mg^{2+} ions dominate the evolution of the crystal morphology with the usual rounding of the (o)/(o) etch pits corner[23,32] (blue box in Figure 5B), and determine the

preferred direction of dissolution. The pinning effect of the adsorbed organic patches further complicates the dissolution process: when a step edge reaches an SA patch, it needs to dissolve laterally in order to avoid the organic layer protecting the edge (blue arrows in Figure 5). Since the SA patches remains intact throughout the process, they can become anchoring points for otherwise unstable calcite terraces despite the dissolution (red arrow in Figure 5E, and Figure S6 for a comparison with Brine1).

Overall, the remarkable stability of SA patches during dilution experiments suggests that the formation of calcium stearate on the surface can be neglected. Had the contrary been true, we would have expected an apparent loss of adsorbed organics during the experiment, in particular during dissolution of the calcite's surface.

3.3 Higher SA coverage on calcite.

Experiments presented in the previous sections demonstrate that organic molecules can form a protecting layer on the surface of calcite and alter its restructuring dynamics, which then takes place in the space around the patches. Here we explore the evolution of calcite with a higher SA coverage and limited gaps between the organic patches. Figure 6 shows the surface of calcite imaged in air one day after the deposition of a high density SA layer. Monoatomic triangular steps typical of freshly cleaved calcite imaged in air are still visible. The ambient humidity usually induces a surface restructuring[58,59] within hours, characterized by the apparition of ~0.3 nm thick hydrated domains (partially visible in Figure 3A). Here, the SA layer appears to prevent, or at least substantially slow down the natural reconstruction process even after a full day of exposure to atmospheric humidity (see also Figure S7). The surface appears homogenous, suggesting a uniform SA coverage, and illustrating the ability of adsorbed organics to act as a protective layer for calcite.

Immersion of the sample in Brine2_×0 triggers an immediate restructuring of the SA layer (Figure 6B-C). Two distinct regions can be identified both in topography and in phase where the SA-coated regions appear higher in topography (Figure 6B) and brighter in phase (Figure 6C) respectively. A profile analysis of these large SA-coated regions indicates that stacked multilayers are present on the surface (Figure S8). A similar restructuring has been previously reported for SA adsorbed on silicon oxide, when placed in contact with an aqueous solution containing Ca^{2+} ions[54]. This suggests a general mechanism for the formation of SA multilayers in the presence of Ca^{2+}, despite possible differences in the SA-surface bond.

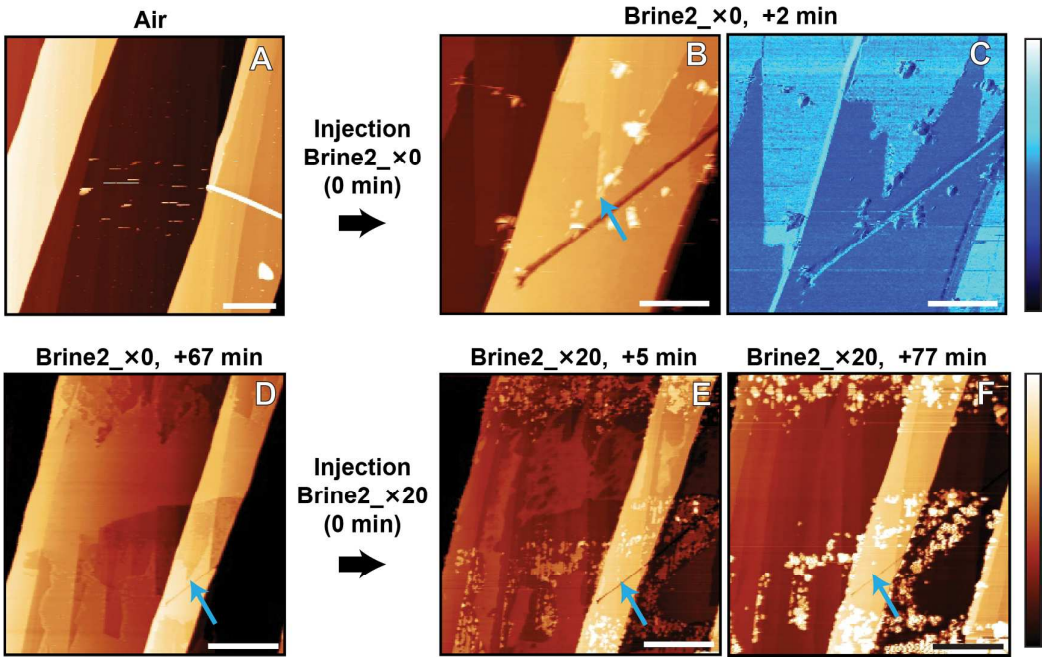

Figure 6: Growth and dissolution of calcite with high SA coverage in Brine2. The surface is first imaged in air (A) and then in Brine2_×0 after 2 min of immersion (B topography and C phase). The phase contrast in (C) reveals the areas covered by an organic layer (brighter) and the bare calcite surface (darker). The same area of the sample imaged 67 min later reveals little changes (D) apart for a topographic contrast reversal due to calcite growth (see text). Diluted Brine2_×20 is subsequently injected and the same area is imaged after 5 min (E) and 77 min (F). The blue arrow points to the tip of a same SA patch in all images. The scale bar is 1 µm (A), 500 nm (B, C), 2 µm (D-F). The color scale bars are 50 nm (A, B, D-F) and 45° (C).

The formation of multilayer stacks 'concentrates' the SA molecules in particular regions of the surface, exposing bare calcite around. After 67 min in the supersaturated Brine2_×0 calcite has grown around the SA stacks and the SA-coated regions initially protruding from the surface (blue arrow in Figure 6B) are now appearing as depression in topography (Figure 6D). The presence of thick organic patches is a direct consequence of the crystal growth, which actively 'pushes' the edges of the initial SA layer to specific confined regions, concentrating the SA molecules and enhancing the formation of multilayers. The process can be observed by following in time a magnified region of Figure 6B (shown in Figure S9). The result of this 'SA concentration' is particularly evident after subsequent dilution of the crystal with unsaturated Brine2_×20, which reveals many thick organic patches on the calcite surface (bright protrusions in Figures 6E-F). These results show that at high organic coverage, the growth of the crystal can strongly affect the organization of the adsorbed organic layer and concentrate the SA molecules into confined regions that are subsequently buried into the crystal.

3.4 General discussion.

The time-lapse AFM images highlight the interplay between the adsorbed SA molecules and the evolving calcite crystal in different brines. This results in a mutual influence of the crystal and the adsorbed organics on their respective molecular organization. The mechanism driving calcite restructuring around the organic molecules could have important implications for several biochemical and geochemical processes, and for the oil industry.

In the case of biochemical and geochemical processes our findings show that the adsorbed fatty acid can modulate not only the intrinsic restructuring dynamics of calcite's surface but also the final thermodynamic equilibrium established between the crystal and the surrounding solution. The presence of adsorbed organics changes the surface roughness and reactivity of the evolving crystal. This is particularly obvious during processes involving competing but energetically dissimilar outcome, for example during directional growth/dissolution of the crystal. During biomineralization, this mechanism could help the organic matrix[12,14] control the direction and growth rate of the calcite shell.

In geophysics, the reduction of the calcite's solubility due to adsorbed fatty acids patches could have implications for the acidification of oceans,[5] a process where the increased atmospheric CO_2 concentration lowers the pH of the oceans causing the dissolution of the $CaCO_3$-based marine organism. Organic-coated calcite would be less likely to dissolve.

In the petroleum industry, the restructuring dynamics of the calcite surface is generally not considered when interpreting so-called imbibition experiments in which a model rock is first exposed to reservoir conditions and then to a situation mimicking water flooding. The growth and dissolution of the calcite crystal could impact the interpretation of such experiments, because it can change both the morphology of the rock and the thermodynamic equilibrium. Additionally, it can influence the history of the rocks, since organic molecules previously trapped in the crystal can be exposed to the solution by progressively decreasing the brine concentration. Our findings could also help explain the important result variability obtained in this kind of experiments. Significantly, results obtained using a more realistic organic deposition method (Supporting Information, section 2) allowed the crystal to restructure around localized SA patches despite large organic aggregates creating a high organic coverage. This observation suggests that in nature, relatively large amounts of organics can become trapped inside calcareous rocks.

Finally, our results highlight the importance of aqueous immersion on the re-organization of adsorbed organic patches, suggesting some caution with experiments evaluating the properties of the deposited organic film using the widely used contact angle or sessile drop technique. The interaction of the liquid with the surface can modify the adsorbed layer and induce an important mismatch between the air and water characterizations.

4. Conclusions

This paper investigated the influence of adsorbed SA molecules on the evolution of calcite $(10\bar{1}4)$ when exposed to different super- and under-saturated brines. Our results show that at low SA coverage, exposure to the brine induces an initial rearrangement of the organic layer with the formation of bilayer or multilayers patches that remain stable on the surface. These patches act as 'pinning points' for the crystal's restructuring surface and slow down any growth or dissolution process. At higher SA coverage, calcite growth tends to concentrate the adsorbed molecules in confined area of the surface, creating thick multilayer patches. When exposed to supersaturated brine, the crystal tends to grow around dense SA patches, incorporating the patches into crystal along with ionic impurities present in the solutions. Subsequent dilution of the brine redissolves the freshly grown material, exposing the SA patches previously incorporated into the crystal during the growth. The proposed interpretation does not take into account calcium stearate that could in principle form in solution from desorbed SA molecules. However, the stability of SA patches during dilution experiments and the absence of unbound surface aggregates suggest that calcium stearate can be neglected here.

These results provide detailed insights into the fate of adsorbed organics at the surface of calcite, and their ability to interfere with the growth and dissolution of the crystal. Carbonate rocks are not static objects but constantly restructure depending on their surroundings, often in the presence of organic material.

Associated content

Supporting Information

Supplementary sections 1-7 comprising the calculations of the SI for each brine dilutions including the different minerals susceptible to form, figures S1-S9 supporting the reported observations with higher resolution details, further discussion and supporting references. This material is available free of charge via the Internet at http://pubs.acs.org.

Author information

*_Corresponding Author_: e-mail: kislon.voitchovsky@durham.ac.uk

§_Present address_: Kemist Institute, Copenhagen University

Author Contributions: Most experiments were conducted by MR with assistance from BE (QNM) and JJS (sample preparation). The manuscript was written with contributions from all authors. All authors have given approval to the final version of the manuscript.

Note: The authors declare no competing financial interests.

Acknowledgments

MR, KV and FS acknowledge financial support from Shell Global Solutions International. The authors thank Bart Suijkerbuijk, Ramez Nasralla and Julija Romanuka (Shell) for useful discussions and for suggesting the brines' composition, and Nianias Nikolaos (EPFL) for proofreading the manuscript. KV acknowledges funding from the Swiss National Science Foundations (Ambizione Fellowship PZ00P2_136941). BE and GF acknowledge financial support from FP7/2007-2013/ERC under Grant Agreement No. 307338, and the Swiss National Science Foundation through Grant No. 205321_134786.

References

(1) Oates, T. *Lime and Limestone*; Kirk-Othmer Encyclopedia of Chemical Technology: Hoboken, NJ, USA, 2000.

(2) Weiner, S.; Addadi, L. Crystallization Pathways in Biomineralization. *Annu. Rev. Mater. Res.* **2011**, *41*, 21–40.

(3) Stanley, S. M. Influence of Seawater Chemistry on Biomineralization Throughout Phanerozoic Time: Paleontological and Experimental Evidence. *Palaeogeogr. Palaeoclimatol. Palaeoecol.* **2006**, *232*, 214–236.

(4) Andersson, A. J.; Mackenzie, F. T.; Bates, N. R. Life on the Margin: Implications of Ocean Acidification on Mg-Calcite, High Latitude and Cold-Water Marine Calcifiers. *Mar. Ecol. Prog. Ser.* **2008**, *373*, 265–273.

(5) Kuffner, I. B.; Andersson, A. J.; Jokiel, P. L.; Rodgers, K. U. S.; Mackenzie, F. T. Decreased Abundance of Crustose Coralline Algae Due to Ocean Acidification. *Nat. Geosci.* **2007**, *1*, 114–117.

(6) Levita, G.; Marchetti, A.; Lazzeri, A. Fracture of Ultrafine Calcium Carbonate/Polypropylene Composites. *Polym. Compos.* **1989**, *10*, 39–43.

(7) Taylor, H. F. W. *Cement Chemistry; 2nd ed.*; Thomas Telford Ltd: London, 1997.

(8) Hartmann, E.; Geckeis, H.; Rabung, T.; Lützenkirchen, J.; Fanghänel, T. Sorption of Radionuclides Onto Natural Clay Rocks. *Radiochim. Acta* **2008**, *96*, 699-707.

(9) Hofmann, S.; Voïtchovsky, K.; Schmidt, M.; Stumpf, T. Trace Concentration – Huge Impact: Nitrate in the Calcite/Eu(III) System. *Geochim. Cosmochim. Acta* **2014**, *125*, 528–538.

(10) Choi, W. H.; Shin, J. W.; Kim, J. J.; Park, J. Y. Calcite-Packed Columns for the Removal of Fluoride in Industrial Wastewater. *Desalin. Water Treat.* **2011**, *30*, 247–253.

(11) Legens, C.; Palermo, T.; Toulhoat, H.; Fafet, A.; Koutsoukos, P. Carbonate Rock Wettability Changes Induced by Organic Compound Adsorption. *J. Petrol. Sci. Eng.* **1998**, *20*, 277–282.

(12) Special Issue on Biomineralization. *Chem. Rev.* **2008**, *108*, 4329–4978.

(13) Thomas, M. M.; Clouse, J. A.; Longo, J. M. Adsorption of Organic Compounds on Carbonate Minerals: 1. Model Compounds and Their Influence on Mineral Wettability. *Chem. Geol.* **1993**, *109*, 201–213.

(14) Smeets, P. J. M.; Cho, K. R.; Kempen, R. G. E.; Sommerdijk, N. A. J. M.; De Yoreo, J. J. Calcium Carbonate Nucleation Driven by Ion Binding in a Biomimetic Matrix Revealed by in Situ Electron Microscopy. *Nat. Mater,* **2015**, *14*, 394–399.

(15) Chen, C.-L.; Qi, J.; Zuckermann, R. N.; DeYoreo, J. J. Engineered Biomimetic Polymers as Tunable Agents for Controlling $CaCO_3$ Mineralization. *J. Am. Chem. Soc.* **2011**, *133*, 5214–5217.

(16) Chukwudeme, E. A.; Hamouda, A. A. Oil Recovery From Polar Components

(Asphaltene and SA) Treated Chalk Rocks by Low Salinity Water and Water Containing SO_4^{2-} And Mg^{2+} At Different Temperatures. *Coll. Surf. A* **2009**, *336*, 174–182.

(17) Karoussi, O.; Hamouda, A. A. Macroscopic and Nanoscale Study of Wettability Alteration of Oil-Wet Calcite Surface in Presence of Magnesium and Sulfate Ions. *J. Colloid Interface Sci.* **2007**, *317*, 26–34.

(18) Romanuka, J.; Hofman, J. P.; Suijkerbuijk, B. M. J. M.; Marcelis, A. H. M.; Oedai, S.; Brussee, N. J.; Van der Linde H A; Aksulu, H.; T, A. *Low Salinity EOR in Carbonates.* SPE Improved Oil Recovery Symposium: Tulsa, Oklahoma, USA, 2012.

(19) Yousef, A. A.; Liu, J.; Al-Saleh, S.; Al-Zahrani, T.; Al-Zahrani, R.; Al-Tammar, H.; Al-Mulhim, N. *SmartWater Flooding: Industry's First Field Test in Carbonate Reservoirs.* SPE international: San Antonio, Texas, USA, 2012.

(20) Mahani, H.; Keya, A. L.; Berg, S.; Bartels, W.-B.; Nasralla, R.; Rossen, W. R. Insights Into the Mechanism of Wettability Alteration by Low-Salinity Flooding (LSF) in Carbonates. *Energ. Fuel.* **2015**, *29*, 1352–1367.

(21) Freij, S. J.; Godelitsas, A.; Putnis, A. Crystal Growth and Dissolution Processes at the Calcite–Water Interface in the Presence of Zinc Ions. *J. Cryst. Growth* **2004**, *273*, 535–545.

(22) De Yoreo, J. J.; Zepeda-Ruiz, L. A.; Friddle, R. W.; Qiu, S. R.; Wasylenki, L. E.; Chernov, A. A.; Gilmer, G. H.; Dove, P. M. Rethinking Classical Crystal Growth Models Through Molecular Scale Insights: Consequences of Kink-Limited Kinetics. *Cryst. Growth Des.* **2009**, *9*, 5135–5144.

(23) Arvidson, R. S.; Collier, M.; Davis, K. J.; Vinson, M. D.; Amonette, J. E.; Luttge, A. Magnesium Inhibition of Calcite Dissolution Kinetics. *Geochim. Cosmochim. Acta* **2005**, *70*, 583–594.

(24) Davis, K. J.; Dove, P. M.; De Yoreo, J. J. The Role of Mg^{2+} as an Impurity in Calcite Growth. *Science* **2000**, *290*, 1134–1137.

(25) Harstad, A. O.; Stipp, S. L. S. Calcite Dissolution: Effects of Trace Cations Naturally Present in Iceland Spar Calcites. *Geochim. Cosmochim. Acta* **2007**, *71*, 56–70.

(26) Agudo, E. R.; Putnis, C. V. Direct Observations of Mineral Fluid Reactions Using Atomic Force Microscopy: the Specific Example of Calcite. *Mineral. Mag.* **2012**, *76*, 227–253.

(27) Gutjahr, A.; Dabringhaus, H.; Lacmann, R. Studies of the Growth and Dissolution Kinetics of the $CaCO_3$ Polymorphs Calcite and Aragonite II. the Influence of Divalent Cation Additives on the Growth and Dissolution Rates. *J. Cryst. Growth* **1996**, *158*, 310–315.

(28) Ruiz-Agudo, E.; Putnis, C. V.; Wang, L.; Putnis, A. Specific Effects of Background Electrolytes on the Kinetics of Step Propagation During Calcite Growth. *Geochim. Cosmochim. Acta* **2011**, *75*, 3803–3814.

(29) Elhadj, S.; De Yoreo, J. J.; Hoyer, J. R.; Dove, P. M. Role of Molecular Charge and Hydrophilicity in Regulating the Kinetics of Crystal Growth. *Proc. Natl. Acad. Sci. USA* **2006**, *103*, 19237–19242.

(30) Hoch, A. R.; Reddy, M. M.; Aiken, G. R. Calcite Crystal Growth Inhibition by Humic Substances with Emphasis on Hydrophobic Acids From the Florida Everglades. *Geochim. Cosmochim. Acta* **2000**, *64*, 61–72.

(31) Orme, C. A.; Noy, A.; Wierzbicki, A.; McBride, M. T.; Grantham, M.; Teng, H. H.; Dove, P. M.; DeYoreo, J. J. Formation of Chiral Morphologies Through Selective Binding of Amino Acids to Calcite Surface Steps. *Nature* **2001**, *411*, 775–779.

(32) Ruiz-Agudo, E.; Putnis, C. V.; Jiménez-López, C.; Rodriguez-Navarro, C. An Atomic Force Microscopy Study of Calcite Dissolution in Saline Solutions: the Role of Magnesium Ions. *Geochim. Cosmochim. Acta* **2009**, *73*, 3201–3217.

(33) Voïtchovsky, K.; Kuna, J. J.; Contera, S. A.; Tosatti, E.; Stellacci, F. Direct Mapping of the Solid-Liquid Adhesion Energy with Subnanometre Resolution. *Nat.*

Nanotechnol. **2010**, *5*, 401–405.
(34) Ricci, M.; Spijker, P.; Voïtchovsky, K. Water-Induced Correlation Between Single Ions Imaged at the Solid--Liquid Interface. *Nat. Commun.* **2014**, *5*, 4400.
(35) De Leeuw, N. H.; Cooper, T. G. A Computer Modeling Study of the Inhibiting Effect of Organic Adsorbates on Calcite Crystal Growth. *Cryst. Growth Des.* **2004**, *4*, 123–133.
(36) Zhang, Y.; Sarma, H. Improving Waterflood Recovery Efficiency in Carbonate Reservoirs Through Salinity Variations and Ionic Exchanges: a Promising Low-Cost "Smart-Waterflood" Approach. SPE international: Abu Dhabi, UAE, 2012.
(37) Parkhurst, D. L.; Appelo, C. A. J. User's Guide to PHREEQC (Version 2): a Computer Program for Speciation, Batch-Reaction, One-Dimensional Transport, and Inverse Geochemical Calculations; 99-4259; Denver, Colorado, 1999.
(38) Cleveland, J. P.; Anczykowski, B.; Schmid, A. E.; Elings, V. B. Energy Dissipation in Tapping-Mode Atomic Force Microscopy. *Appl. Phys. Lett.* **1998**, *72*, 2613–2615.
(39) Voïtchovsky, K. Anharmonicity, Solvation Forces, and Resolution in Atomic Force Microscopy at the Solid-Liquid Interface. *Phys. Rev. E* **2013**, *88*, 022407EP.
(40) Garcia, R.; Gómez, C.; Martinez, N.; Patil, S.; Dietz, C.; Magerle, R. Identification of Nanoscale Dissipation Processes by Dynamic Atomic Force Microscopy. *Phys. Rev. Lett.* **2006**, *97*, 016103.
(41) Ricci, M.; Spijker, P.; Stellacci, F.; Molinari, J.-F.; Voïtchovsky, K. Direct Visualization of Single Ions in the Stern Layer of Calcite. *Langmuir* **2013**, *29*, 2207–2216.
(42) Voïtchovsky, K.; Ricci, M.; High-Resolution Imaging of Solvation Structures with Amplitude-Modulation Atomic Force Microscopy. *SPIE BiOS*, **2012**; 8232, 82320O–82320O-8
(43) Melcher, J.; Carolina Carrascob, C.; Xua, X.; Carrascosad, J. L.; Gomez-Herrerob, J.; de Pablob, P. J.; Raman, A. Origins of Phase Contrast in the Atomic Force Microscope in Liquids. *PNAS* **2009**, 1–6.
(44) Kiracofe, D.; Raman, A. Nonlinear Dynamics of the Atomic Force Microscope at the Liquid-Solid Interface. *Phys. Rev. B* **2012**, *86*, 205405EP.
(45) Hutter, J. L.; Bechhoefer, J. Calibration of Atomic-Force Microscope Tips. *Rev. Sci. Instrum.* **1993**, *64*, 1868–1873.
(46) Adamcik, J.; Berquand, A.; Mezzenga, R. Single-Step Direct Measurement of Amyloid Fibrils Stiffness by Peak Force Quantitative Nanomechanical Atomic Force Microscopy. *Appl. Phys. Lett.* **2011**, *98*, 193701.
(47) Pittenger, B.; Slade, A. Performing Quantitative Nanomechanical AFM Measurements on Live Cells. *Microscopy Today* **2013***, 21,* 12-17.
(48) Zhang, S.; Aslan, H.; Besenbacher, F.; Dong, M. Quantitative biomolecular imaging by dynamic nanomechanical mapping. *Chem. Soc. Rev.* **2014**, *43*, 7412-7429.
(49) Wasylenki, L. E.; Dove, P. M.; Wilson, D. S.; De Yoreo, J. J. Nanoscale Effects of Strontium on Calcite Growth: an in Situ AFM Study in the Absence of Vital Effects. *Geochim. Cosmochim. Acta* **2005**, *69*, 3017–3027.
(50) O'brien, W. J.; Hermann, J. J. The Strength of Liquid Bridges Between Dissimilar Materials. *J. Adhesion* **1973**, *5*, 91–103.
(51) Fenter, P.; Sturchio, N. C. Structure and Growth of Stearate Monolayers on Calcite: First Results of an in Situ X-Ray Reflectivity Study. *Geochim. Cosmochim. Acta* **1999**, *63*, 3145–3152.
(52) Sauthier, G.; Segura, J. J.; Fraxedas, J.; Verdaguer, A. Hydrophobic Coating of Mica by Stearic Acid Vapor Deposition. *Colloids Surf. A* **2014**, *443*, 331–337.
(53) Mihajlović, S. R.; Vučinić, D. R.; Sekulić, Ž. T.; Milićević, S. Z.; Kolonja, B. M. Mechanism of Stearic Acid Adsorption to Calcite. *Powder Technol.* **2013**, *245*, 208–216.
(54) Kumar, N.; Wang, L.; Siretanu, I.; Duits, M.; Mugele, F. Salt Dependent Stability of Stearic Acid Langmuir–Blodgett Films Exposed to Aqueous Electrolytes. *Langmuir* **2013**, *29*, 5150–5159.

(55) Aschauer, U.; Spagnoli, D.; Bowen, P.; Parker, S. C. Growth Modification of Seeded Calcite Using Carboxylic Acids: Atomistic Simulations. *J. Coll. Interf. Sci.* **2010**, *346*, 226–231.
(56) Hillner, P. E.; Gratz, A. J.; Manne, S.; Hansma, P. K. Atomic-Scale Imaging of Calcite Growth and Dissolution in Real Time. *Geology* **1992**, *20*, 359–362.
(57) Vavouraki, A. I.; Putnis, C. V.; Putnis, A.; Koutsoukos, P. G. An Atomic Force Microscopy Study of the Growth of Calcite in the Presence of Sodium Sulfate. *Chem. Geol.* **2008**, *253*, 243–251.
(58) Stipp, S. L. S.; Gutmannsbauer, W.; Lehmann, T. The Dynamic Nature of Calcite Surfaces in Air. *Am. Mineral.* **1996**, *81*, 1–8.
(59) Baltrusaitis, J.; Grassian, V. H. Calcite (1014) Surface in Humid Environments. *Surf. Sci.* **2009**, *603*, L99–L104.

Table of Content/Abstract Graphic